Mass Spectrometric Analysis of Nonequilibrium Airflows

WILLIAM N. MACDERMOTT* AND RICHARD E. DIX†
ARO Inc., Arnold Engineering Development Center, Arnold Air Force Station, Tenn.

Comprehensive measurements were made of the nonequilibrium chemical composition of arc-heated air expanding from reservoir temperatures and pressures of 2120 to 5380°K and 3.7 to 20.8 atm, respectively. A sampling probe containing a quadrupole mass spectrometer and a cryopump was used. Flow composition varied systematically with reservoir entropy, ranging from "normal" air to a highly nonequilibrium mixture containing 25% atomic oxygen and 8% nitric oxide. At low entropy, measured compositions compared favorably with finite-rate theory, but significant disagreement was evident at high entropy. Possible modifications to accepted reaction rates were investigated.

Introduction

RAPID expansion of high enthalpy gases in converging-diverging nozzles generally results in some degree of chemical nonequilibrium. Theories exist which account for chemical reactions and vibrational energy exchanges proceeding at finite rates under the influence of rapidly changing thermodynamic variables in such flows. These theories are assembled from a large number of individual assumptions as to the species and reactions of importance in the flow, the rate equations applicable, the chemical and vibrational rate constants to be used, and the degree of coupling of the chemical and vibrational processes. Since the number and quality of independent measurements required to unambiguously define the state of a complex nonequilibrium gas exceeds existing measurement capability, experimental demonstrations that nonequilibrium airflows actually behave as predicted by finite rate calculations are incomplete.

Limited demonstrations that some measured variables in nonequilibrium airflows follow the predictions of finite rate calculations were given initially by conventional measurements of static pressure, Pitot pressure, and local mass flux.[1-3] A more comprehensive demonstration was provided by development of the electron beam as a diagnostic tool, since static (rotational) temperature, vibrational temperature, and static density were added to the group of measurable variables in the flow. The correlation of nonequilibrium effects with reservoir entropy, first observed in theoretical calculations, was demonstrated experimentally by an electron beam experiment which covered the transition from near-equilibrium to near-frozen flow.[4,5]

It is not obvious that successful prediction of nonequilibrium behavior of thermodynamic variables will necessarily be accompanied by comparable accuracy in prediction of the chemical composition. Chemical calibration of nonequilibrium flows, however, has proved to be even more difficult than thermodynamic calibration. At least three different techniques have been applied to this problem: optical spectroscopy, catalytic probes, and mass spectrometry. Of the three, mass spectrometry offers the broadest capability, but early attempts at application in flowing gases were not notably successful. The main problems appeared to lie in the aerodynamics of obtaining an undisturbed sample of the flow.

In the study reported herein, the requirements for sampling in place were recognized to be a mass spectrometer compact enough to fit within a small sampling probe, and a pumping system capable of maintaining the pressure within the probe at 10^{-4} torr or less. These requirements were met by a quadrupole mass spectrometer and a liquid-hydrogen cryopump. Basic development and feasibility tests with such a probe were reported in Ref. 6. Subsequently, the performance of the mass spectrometer was improved, and significant advances in understanding the nature of its outputs were made. Experimental determinations of chemical compositions in nonequilibrium airflows have been made that are at least as comprehensive as the thermodynamic measurements of Ref. 5 and appear to be equally successful. The increased capability of the instrument allowed systematic experimental determination of both NO and atomic oxygen concentrations and demonstration of the correlation of chemical composition with entropy.[7]

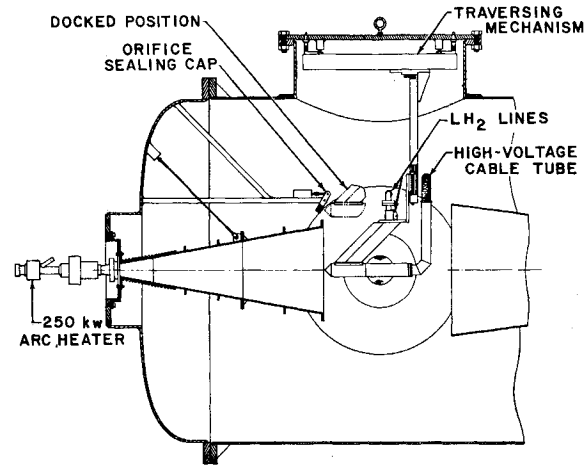

Fig. 1 The 18-in. low-density wind tunnel.

Description of Test Apparatus

Wind Tunnel

The nonequilibrium air expansions that were subjected to mass spectrometric analysis were produced in an arc-heated low-density wind tunnel, Fig. 1. A small stilling chamber was located downstream of a 250 kw d.c. arc heater to serve as a reservoir for a conical nozzle exhausting into an open-jet test section. The test section was continuously evacuated with a six-stage steam ejector. The dimensions of the nozzle were: a throat diameter of 0.200 in., an exit diameter of 18 in., a conical half-angle of 10°, and a geometric exit-to-throat area ratio of 8100. Reservoir conditions produced for this test included stagnation pressures of 3.74–20.9 atm, stagnation temperatures of 2120–5380°K, and dimensionless entropy in the reservoir (S/R) from 29.4 to 37.83. Conditions in the nozzle reservoir were determined by the energy balance technique, requiring accurate measurements of heater input power, air mass flow, and power absorbed by the cooling water in all cooling

Presented as Paper 71-621 at the AIAA 4th Fluid and Plasma Dynamics Conference, Palo Alto, Calif., June 21–23, 1971; submitted July 19, 1971; revision received November 1, 1971. The research reported herein was sponsored by the Arnold Engineering Development Center, Air Force Systems Command, under Contract F40600-71-C-0002 with ARO Inc. Further reproduction is authorized to satisfy needs of the U.S. Government.

Index categories: Reactive Flows; Rarefied Flows.

* Supervisor, Analysis Section, Pilot Tunnels Branch, Propulsion Wind Tunnel.

† Research Engineer, 4T Projects Branch, Propulsion Wind Tunnel. Member AIAA.

passages up to the throat. In the expanded flows at the nozzle exit, static pressure varied from 10×10^{-3} to 30×10^{-3} torr, and static temperature varied from 50 to 140°K, as reported in the detailed study of Refs. 4 and 5.

Chemical composition was expected to be frozen well upstream of the nozzle exit and, hence, a function of reservoir conditions only. There was, therefore, no reason to repeat the extensive measurements of thermodynamic variables in the test section.

Mass Spectrometer Probe

Only recently have mass spectrometers become available in a size small enough for usefulness in probe studies of aerodynamic flows. A quadrupole type was selected for this research, 4.5 cm diam and 24 cm long, with high resolution and sweep times of a second or better. This type of mass spectrometer accomplishes mass discrimination through the influence on ion trajectory of an oscillating electrical field of four poles. Ions surviving the separation process are detected as a function of time by an electron multiplier.

The sampling probe in which the spectrometer was mounted was a cone-cylinder supported by a strut attached to a traversing mechanism with vertical and streamwise degrees of freedom, Fig. 2. The probe was water cooled where required to ensure survival, and electrical operating and signal leads were protectively routed to ensure proper operation of the quadrupole. The sampling orifice at the tip of the cone had a diameter of 0.0254 cm, resulting in an orifice Knudsen number of 0.9–5.0 for the range of operating conditions investigated. A self-contained cryopump was designed to maintain the 10^{-4} torr environment required for proper operation of the mass spectrometer. Liquid hydrogen was selected as the cryogen because of the need to pump all of the gases of interest in arc-heated airflow studies, and because of low-cost availability. An auxiliary mechanical pump was used to evacuate the interior of the probe to about 10^{-2} torr prior to filling the liquid hydrogen cryopump.

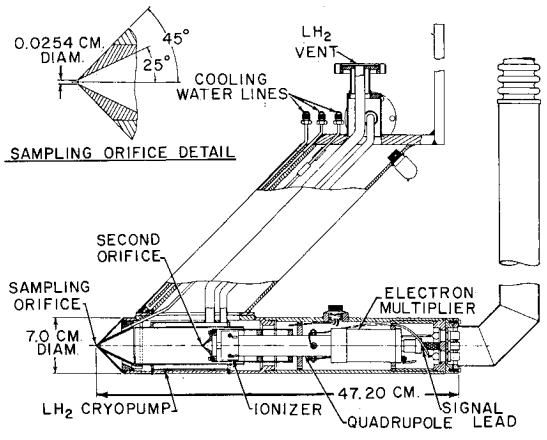

Fig. 2 Cross section of the mass spectrometer probe.

Calibration of the Mass Spectrometer

It was quickly determined during operation of the mass spectrometer in a static test chamber that absolute outputs were not sufficiently repeatable for use in quantitative analysis of the wind-tunnel mixtures. On plots of output sensitivity vs electron energy, hysteresis loops spanning two orders of magnitude in absolute sensitivity were observed, depending upon the state of contamination of the mass spectrometer ionizer. Relative sensitivity to various mass number particles, however, was found to be much more reliable. Relative output sensitivity of simple undissociated ions displayed good repeatability ($\pm 1\%$) in a clean system, and acceptable repeatability ($\pm 4\%$) in a grossly contaminated system. Relative sensitivity of dissociated ions was repeatable to $\pm 4\%$ in a clean system, but in a contaminated system, only to within an order of magnitude. Thus, even when obtaining from the spectrometer only relative outputs, the state of contamination required continuous monitoring. Calibration of the relative sensitivities of the spectrometer was performed in a static test chamber, using various prepared mixtures of multicomponent gases. Relative sensitivities of the spectrometer to gas components that could not be prepared in stable mixtures at room temperature; i.e., atomic oxygen and nitrogen, were obtained by reference to values of ionization cross section reported in scientific literature.[7]

The ion detector provided as standard equipment with the mass spectrometer was found to be far too sensitive to contamination for operation in the severe environment of the arc wind tunnel. To achieve stable calibrations it was necessary to substitute a magnetic electron multiplier of the resistance strip type.

Test Procedure

It was not considered necessary to establish test conditions at constant values of either reservoir pressure or temperature, since the results of Ref. 8 suggestd the nonequilibrium composition would correlate with reservoir entropy alone. Stagnation pressures from 3.7 to 20.8 atm and temperatures from 2120 to 5380°K were obtained, covering a range in reservoir entropy from $S/R = 29.5$ to $S/R = 37.8$.

Prior to a test run, the test section was evacuated to about 10^{-2} torr with the steam ejector, during which time the probe, in the docked and capped position (Fig. 1), was evacuated with a mechanical pump to approximately 10^{-2} torr. Cooling water, liquid hydrogen, and air flows were then established and the arc ignited. When flow conditions were established, the probe cap was removed using a hydraulic actuator, and the probe traversed to the desired station in the flow. After recording mass spectra, the probe was retracted and capped. Exposure of the probe to the flow lasted from 3 min to 8 min, determined by heating of the probe at the forward O-ring seal.

Although the arc-heater operation was generally stable, short-lived high-frequency random fluctuations in arc-heater voltage and current did occur, and were probably responsible for some simultaneously observed fluctuations in mass abundances, particularly at the m/e ratios corresponding to the high temperature components, NO and O. Because of these possible output fluctuations, an oscilloscope was used to monitor the spectrum continuously, and when desired, a direct-write oscillograph was triggered to record several spectra for each data point to assure statistically valid abundances. During the period of a typical average spectrum, about 6–8 sec., fluctuations of $\pm 20\%$ were observed in NO and O, while the N_2 and O_2 outputs changed only about $\pm 7\%$.

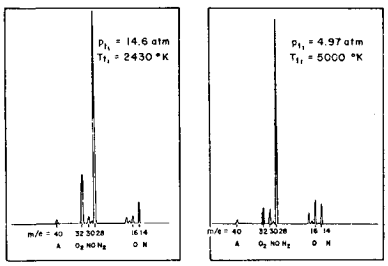

Fig. 3 Mass spectra obtained in wind tunnel.

Test Results

Typical Spectra

The finite-rate expansion calculations predict, for increasing stagnation temperature, an O_2 concentration decreasing with respect to N_2, increasing N and O concentrations, and a peaking behavior of NO. Two typical mass spectra are given in Fig. 3 for both high and low stagnation temperatures. The decrease in O_2 and increase in O and NO relative to N_2 is evident at

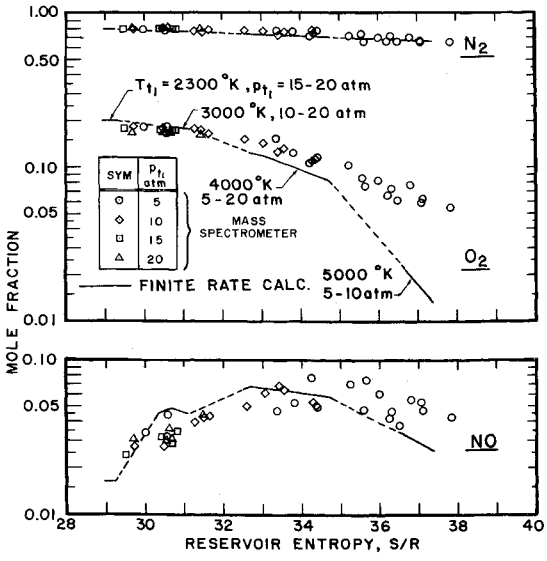

Fig. 4 Comparison of experimental and theoretical compositions in the 18-in. wind tunnel, molecular species.

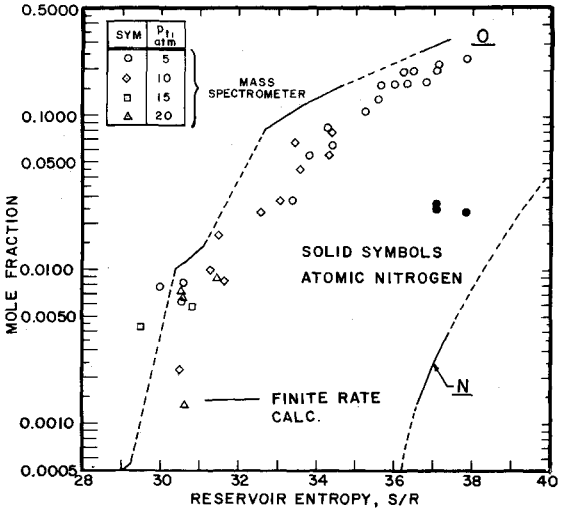

Fig. 5 Comparison of experimental and theoretical compositions in the 18-in. wind tunnel, atomic species.

the higher temperatures. The appreciable output signal at mass number 14 is spurious since it comes predominantly from dissociation of N_2 within the ionizer section of the mass spectrometer. When this contribution is subtracted from the total $m/e = 14$ signal using calibration data obtained in a static test chamber, very little signal remains attributable to atomic nitrogen in the sampled gas. This is in qualitative agreement with the finite-rate calculations that predict less than 0.003 mole fraction of atomic nitrogen for the above range of test conditions. On the other hand, the output signal at $m/e = 16$ for the 5000°K stagnation temperature represents almost entirely atomic oxygen in the sample. (Calibration data indicate that only 10% of the already small signal at $m/e = 32$ would contribute to the signal at $m/e = 16$ through dissociative ionization of O_2 in the spectrometer ionizer.)

Entropy Correlation

As just cited, the data of Ref. 8 indicate that a correlation exists between nonequilibrium compositions calculated by finite-rate theory, and reservoir entropy. The experimental measurements described herein also fit this scheme. All of the mass spectra data for the molecular species, N_2, NO, and O_2, are given in Fig. 4. Data for the atomic species, N and O, are given in Fig. 5. Experimental points are identified with respect to the nominal value of stagnation pressure. Each point represents an average over at least six mass spectra during a single run

Table 1 Reactions included in finite rate model

Reaction	C_1	C_2	C_3	n
$O_2+O_2 \rightleftarrows 2O+O_2$	8.0×10^{13}	$-3/2$	0	2
$O_2+O \rightleftarrows 2O+O$	2.3×10^{14}	$-3/2$	0	2
$O_2+N_2 \rightleftarrows 2O+N_2$	6.2×10^{9}	$-1/2$	0	2
$O_2+N \rightleftarrows 2O+N$	3.0×10^{9}	$-1/2$	0	2
$O_2+NO \rightleftarrows 2O+NO$	3.0×10^{9}	$-1/2$	0	2
$N_2+O_2 \rightleftarrows 2N+O_2$	1.1×10^{10}	$-1/2$	0	2
$N_2+O \rightleftarrows 2N+O$	1.1×10^{10}	$-1/2$	0	2
$N_2+N_2 \rightleftarrows 2N+N_2$	2.8×10^{10}	$-1/2$	0	2
$N_2+N \rightleftarrows 2N+N$	2.4×10^{15}	$-3/2$	0	2
$N_2+NO \rightleftarrows 2N+NO$	1.1×10^{10}	$-1/2$	0	2
$NO+O_2 \rightleftarrows N+O+O_2$	1.0×10^{14}	$-3/2$	0	2
$NO+O \rightleftarrows N+O+O$	1.0×10^{14}	$-3/2$	0	2
$NO+N_2 \rightleftarrows N+O+N_2$	1.0×10^{14}	$-3/2$	0	2
$NO+N \rightleftarrows N+O+N$	1.0×10^{14}	$-3/2$	0	2
$NO+NO \rightleftarrows N+O+NO$	2.0×10^{15}	$-3/2$	0	2
$O+N_2 \rightleftarrows NO+N$	1.6×10^{10}	0	0	1
$NO+O \rightleftarrows N+O_2$	1.3×10^{7}	1	$-3{,}560$	1
$N_2+O_2 \rightleftarrows 2NO$	2.4×10^{20}	$-5/2$	$-43{,}000$	1

Reverse reaction rate constant:

$$k_r = C_1 T^{C_2} \exp\left(\frac{C_3}{T}\right), \quad \left(\frac{\text{m}^3}{\text{kg mole}}\right)^n \frac{1}{\text{sec}}$$

at stabilized arc-heater conditions. All points were obtained in the inviscid test core at distances from 2 in. to 3 in. from the nozzle centerline. Test data were corrected for the effects of ionizer dissociation at $m/e = 14$ and 16, and mass separation or migration within the sampling probe.

The broken line curves of Fig. 4 represent the results of the finite rate calculations described in Ref. 5. These results are in close agreement with the entropy correlation of Ref. 8, except for NO at $S/R > 33.0$. The calculations of Ref. 5 represent a simultaneous solution of the gas dynamic flow equations, the chemical rate equations, and vibrational energy relaxation equations. Air was considered to be a mixture of only five species, N, O, N_2, NO, and O_2. The energetically-important dissociation/recombination reactions for N_2, NO, and O_2, as well as the NO shuffle reactions, were included in a system of eighteen coupled finite-rate chemical reaction equations listed in Table 1. Finite-rate vibrational energy exchanges were included for the three diatomic molecules. The thermodynamic predictions based on this theory were satisfactorily verified by electron beam measurement.[5] The solid line segments of the theoretical curves represent the finite-rate solutions at constant stagnation temperatures of 2300, 3000, 4000, and 5000°K. The dashed lines are simply fairings of the theoretical values between the constant temperature segments.

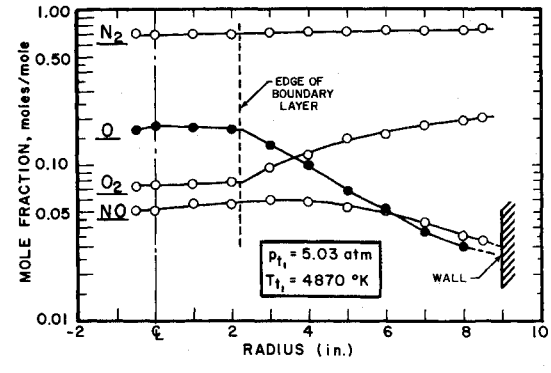

Fig. 6 Boundary-layer composition

Boundary-Layer Measurements

A limited number of composition measurements in the boundary layer were obtained by point-to-point traverses over the entire upper half of the nozzle exit flow. A sample distribution of species concentrations for such a traverse is given

in Fig. 6 for a stagnation pressure of 5.03 atm and a stagnation temperature of 4870°K. The composition was essentially constant in the inviscid core, but varied systematically through the boundary layer.

Discussion

General

The first impression to be gained by examination of the experimental composition data of Figs. 4 and 5 is that a systematic correlation with the entropy parameter indeed exists. The cluster of test points at $S/R = 30.5$ is notable, since the compositions are essentially repeated for a wide range of reservoir pressure and temperature. This correlation of frozen composition is of considerable value in analyzing and organizing the chemical nonequilibrium effects in wind-tinnel nozzle flows.

The second impression to be gained is that the general trends predicted by theory are confirmed experimentally, in particular the peaking behavior of the nitric oxide fraction. Concentrations of the three molecular species, N_2, NO, and O_2, together contributing over 85% of the total sample, are in close quantitative agreement with finite-rate predictions at S/R less than 32. Above $S/R = 32$, there is a divergence, with the O_2 fraction exceeding the theoretical value by 6 to 7% of the total sample and the NO fraction reaching a value approximately 3% greater than predicted. Aside from these differences, the molecular data are very consistent over the given entropy range and tend to display the same general shapes as do the theoretical curves.

The two atomic fractions, N and O, are not in so good agreement with the theory. The calculations indicate the atomic nitrogen fraction is negligible, below the 0.003 detectability limit for the given range of reservoir entropy. The measurements confirm this, for the most part, although there were sporadic indications of N during a few separate runs at high stagnation temperature, Fig. 5. It is not certain whether these were valid detections or simply the result of inaccuracies in applying the dissociative ionization correction to the output signal at $m/e = 14$.

The atomic oxygen fractions, however, were readily detected, and ranged from the lower detectability limit to approximately 0.23 mole fraction at the highest entropy. Although the atomic oxygen measurements were self-consistent they were lower than the theoretical calculations, by 0.5–9% of the total sample. (In relation to the predicted 0 fraction, however, the average discrepancy is 30–60%.)

Possible Explanations of Discrepancies Berween Measured and Calculated Compositions

There are three possible explanations of the discrepancies noted previously. The possibility of lighter particle migration in the low-density nozzle expansion is suggested because of the indicated reduced concentrations of light species and increased concentrations of heavy species near the center of the jet. However, the composition data for the boundary layer, Fig. 6, show not only a constant composition over the entire viscous core, but actually display a decreasing concentration of the lightest component, O, away from the axis of the flow, presumably because of recombination in the boundary layer.

The second class of explanations involves critical evaluation of the influence of the mass spectrometer. Mass separation inside the probe was included in the data reduction process through the assumption of free molecular diffusion of flow particles away from the sampled stream tube prior to entering the ionizer of the mass spectrometer. Since, for each of the i species the velocity of diffusion is inversely proportional to the square root of the molecular weight, $(M_i)^{-1/2}$, the flux per unit area of the ith species at the ionizer inlet aperture was reduced from that at the probe inlet orifice by a factor proportional to M_i. The relative sensitivities of the mass spectrometer system for the molecular species N_2, NO, and O_2 were established through direct calibrations that were repeatable within a few percent under controlled conditions of cleanliness. It was not possible to similarly calibrate the relative sensitivities to N and O, however, so published values of ionization cross sections for N and O atoms under electronic bombardment were resorted to.[7] The accuracy of these cross sections is difficult to judge; however, it is noted that the varying discrepancy between measured and predicted O fractions, Fig. 5, is not consistent with a constant percentage error in relative sensitivity of the mass spectrometer probe system to atomic oxygen, as would result from erroneous cross sections.

More probable bases for explaining the discrepancies appear within the finite-rate calculations. There is evidence from other types of experiments that the discrepancy in the O/O_2 system is real. In a recent catalytic probe experiment,[9] measured atomic oxygen concentrations in a shock tunnel expansion were found to be much lower than predicted by a finite rate calculation using reaction rates differing from those of Table 1 by no more than a factor of 4 (except for NO dissoiation by third bodies other than NO). A similar result has been obtained from observations of oxygen components of radiation from an electron beam in a steady-state nonequilibrium airflow.[10]

The kinetic rate data used in the chemical model, Table 1, were cited by Gavril[11] from an original summary by Steiger.[12] Based on the behavior of theoretical finite-rate solutions, it was concluded by Lordi and Mates[13] that the nitrogen and nitric oxide concentrations in finite-rate expansions of air were determined almost entirely by the fast (two-body) nitric oxide shuffle reactions (Nos. 16 and 17, Table 1), while the oxygen concentration was determined principally by the slower (three-body) oxygen dissociation/recombination reactions (Nos. 1–5, Table 1). If this conclusion is considered in conjunction with the present experimental results that show discrepancies not in the N_2/NO system, but rather in the O/O_2 system, then it can be postulated that the rates of the two shuffle reactions are known much more accurately than those for the oxygen three-body reactions. A summary of reaction rate data by Bortner[14] indicates indeed that the original experimental data for the shuffle reactions are much more consistent over an extensive range of temperature than are any of the corresponding data for the termolecular reactions.

In fact, the original experimental data for the dissociation-recombination reactions appear to be in a highly unsatisfactory state. Although reasonable agreement exists between measurements of many different investigators for a given reaction and a given temperature range, there is nearly universal disagreement between the high- and low-temperature measurements for a given reaction. Dissociation rates at high temperature, converted to recombination rates by the equilibrium constant and extrapolated to low temperatures, disagree with measured low-temperature recombination rates by up to two orders of magnitude.[14] Further, the empirical fits to the experimental data over the complete temperature range of interest result in pre-exponential factors in the reaction rate constants that are larger than the molecular collision rates at low temperatures. These discrepancies are sufficiently serious that basic misinterpretations of the measurements have been suggested: either the reactions involved are more complex than the simple single-step reactions assumed; the recombination process changes character with temperature; or the influence of excited states of the reactants is more important than assumed.[14]

The dissociation rate in a typical nonequilibrium expansion of air rapidly decreases to negligible levels because of the exponential dependence on temperature. As a result, the final frozen O/O_2 composition is controlled mainly by the rate of the recombination reaction at temperatures near the sonic part of the expansion. In this range the rate data are based on dissociation rate measurements in shock tubes in which the chemical relaxation is from low to high temperature. Thus, there appears to be a striking parallel with the case of vibrational relaxation. It was determined a number of years ago that the vibrational rates measured in relaxation from low to high temperature in a shock tube are much slower than vibrational rates of relaxation which occur in rapid nozzle expansions where the direction of relaxation is in the opposite sense, i.e., from high temperature to low temperature.[15,16]

Another possible perturbation to the reaction rates was the presence of potential catalysts in the form of metallic vapors in the flow. Erosion of the arc heater electrodes, particularly at high enthalpy, introduced small quantities of copper and silver which were detectable on a qualitative basis by the mass spectrometer probe. A determination of the importance of these contaminants was beyond the scope of this study.

A short study was made to determine the magnitude of oxygen reaction rates that would reduce or eliminate the discrepancy in the O/O_2 compositions. Additional finite-rate calculations were performed with the reaction rates of the first five reactions of Table 1 increased by factors of 10 and 100. These calculations were made for only two reservoir conditions: 10 atm, 4000°K, and $S/R = 33.6$; and 5 atm, 5000°K, and $S/R = 37.0$. The results of these calculations are given in Figs. 7 and 8, superimposed on the bands of experimental data from Figs. 4 and 5. Curves have been faired through the calculated points approximately parallel to the curves for the original calculations. It is noted that the experimental/theoretical discrepancy could be eliminated for oxygen rate magnifications between 10 and 100.

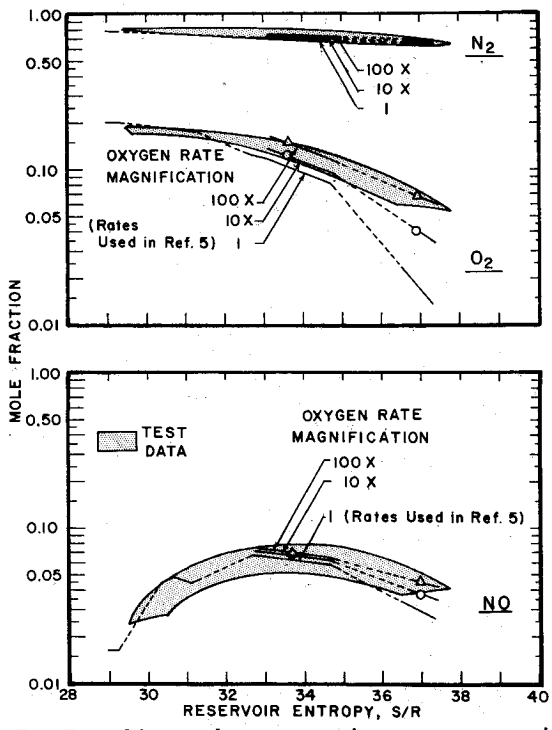

Fig. 7 Effect of increased oxygen reaction rates on comparison of experimental and theoretical compositions, molecular species.

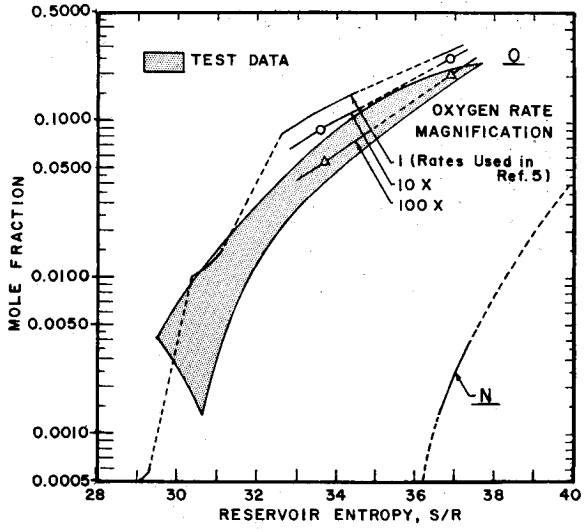

Fig. 8 Effect of increased oxygen reaction rates on comparison of experimental and theoretical compositions, atomic species.

Conclusions

1) A mass spectrometer sampling probe was developed to make possible in situ determination of the chemical composition in nonequilibrium flowing gases. Experimental repeatability was observed to be within 1–4% when determining relative concentrations of molecular species, and 4–10% when determining relative composition of atomic species. Repeatability of determinations of absolute species concentrations was observed to be quite poor.

2) Frozen compositions in a low-density expansion of air in an arc-heated wind tunnel were determined for reservoir pressures of 3.7–20.8 atm and reservoir temperatures of 2120–5380°K. Both molecular and atomic compositions determined experimentally were correlated with reservoir entropy. The molecular species concentrations agreed with finite-rate calculations at low entropy, but diverged by as much as 7% at high entropy. The atomic oxygen concentration was consistently less than predicted values over the entire entropy range, and at the highest entropy it was 9% less than expected.

3) Oxygen reaction rate increases of 10–100 times previously accepted values were required to bring the predicted concentrations of O and O_2 into agreement with the concentrations observed in the wind-tunnel flow. The much better agreement with theory of the nitrogen and nitric oxide concentrations is considered to be evidence of a high degree of accuracy in the rates used for the nitric oxide shuffle reactions.

4) It is considered that the most probable explanation of the discrepancy between predicted and experimental oxygen concentrations is the reliance in theoretical calculations upon high temperature three-body recombination rates for oxygen that are not substantiated by direct experiments, but are derived from high temperature dissociation rates.

5) Flow composition was determined in the nozzle boundary layer for a limited number of cases. Composition varied little across the inviscid core, but considerable variation was detected in species concentrations in the boundary layer, always in the direction of recombination, as expected.

References

[1] Nagamatsu, H. T. and Sheer, R. E., "Vibrational Relaxation and Recombination of Nitrogen and Air in Hypersonic Nozzle Flows," *AIAA Journal*, Vol. 3, No. 8, Aug. 1964, pp. 1386–1391.

[2] Duffy, R. E., "Experimental Study of Nonequilibrium Expanding Flows," *AIAA Journal*, Vol. 3, No. 2, Feb. 1965, pp. 237–244.

[3] Zonars, D., "Nonequilibrium Regime of Airflows in Contoured Nozzles: Theory and Experiments," *AIAA Journal*, Vol. 5, No. 1, Jan. 1967, pp. 57–63.

[4] MacDermott, W. N. and Marshall, J. C., "Theoretical and Experimental Nonequilibrium Expansions of Partially-Dissociated Air," AIAA Paper 69-328, Cincinnati, Ohio, 1969.

[5] MacDermott, W. N. and Marshall, J. C., "Nonequilibrium Nozzle Expansions of Partially Dissociated Air: A Comparison of Theory and Electron-Beam Measurements," AEDC-TR-69-66 (AD690493), July 1969, Arnold Engineering Development Center, Arnold Air Force Station, Tenn.

[6] Dix, R. E., "Sampling Probe for Instantaneous Mass Spectrometric Analysis of Rarefied High Enthalpy Flow," AEDC-TR-69-37 (AD686405), March 1969, Arnold Engineering Development Center, Arnold Air Force Station, Tenn.

[7] MacDermott, W. N. and Dix, R. E., "Final Results of On-Line Mass Spectrometric Analysis of Nonequilibrium Airflows," AEDC-TR-71-23, Feb. 1971, Arnold Engineering Development Center, Arnold Air Force Station, Tenn.

[8] Harris, C. J., "Comment on Nonequilibrium Effects on High-Enthalpy Expansion of Air," *AIAA Journal*, Vol. 4, No. 6, June 1966, pp. 1148–1149.

[9] Bartz, J. A. and Vidal, R. J., "Research on Surface Catalysis in Nonequilibrium Flows," AEDC-TR-70-11 (AD704814), April 1970, Arnold Engineering Development Center, Arnold Air Force Station, Tenn.

[10] Petrie, S. L., Boiarski, A. A., and Lazdinis, S. S., "Electron Beam Studies of Molecular and Atomic Oxygen in Nonequilibrium Flows," AIAA Paper 71-271, Albuquerque, N. Mex., 1971.

[11] Gavril, B. D., "Generalized One-Dimensional Chemically Reacting Flows with Molecular Vibrational Relaxation," TR 426 (AD435623),

Jan. 1964, General Applied Science Labs. Inc.
[12] Steiger, M. H., "On the Chemistry of Air at High Temperatures," Rept. TR-357, Jan. 1963, General Applied Science Labs. Inc.
[13] Lordi, J. A. and Mates, R. E., "Nonequilibrium Expansions of High Enthalpy Airflows," ARL 64-206, Nov. 1964, Aerospace Research Labs., Wright-Patterson Air Force Base, Ohio.
[14] Bortner, M. H., "A Review of Rate Constants of Selected Reactions of Interest in Re-Entry Flow Fields in the Atmosphere," TN 484, May 1969, National Bureau of Standards.
[15] Hurle, I. R., Russo, A. L., and Hall, J. G., "Spectroscopic Studies of Vibrational Nonequilibrium in Supersonic Nozzle Flows," ARL-65-6, Jan. 1965, Aerospace Research Labs., Wright-Patterson Air Force Base, Ohio.
[16] Sebacher, D. I., "A Correlation of N_2 Vibrational-Translational Relaxation Times," *AIAA Journal*, Vol. 5, No. 4, April 1967, pp. 819–820.

APRIL 1972 AIAA JOURNAL VOL. 10, NO. 4

Laminar Boundary Layers Developed within Unsteady Expansion and Compression Waves

J. GORDON HALL*
State University of New York at Buffalo, Buffalo, N. Y.

The paper analyzes unsteady laminar wall boundary layers formed within centered compression or expansion waves traveling into gas at rest, and also the resultant displacement effects on inviscid flow in a tube. For the boundary layer, a previous analysis by Cohen is generalized to include both compression and expansion flows and allow for wall surface temperature change as occurs with finite wall thermal conductivity. Solutions obtained by coordinate expansions show that at higher pressures the wall surface temperature change significantly reduces surface heat transfer, outweighing higher order effects of the previous analysis for wall temperature constant. For the displacement effect, the method of characteristics is used to obtain linearized solutions. Characteristic features of the boundary layer and its displacement effect on inviscid tube flow are compared for compression and expansion wave flows. For either type of wave, boundary-layer displacement acts to diminish the basic inviscid-flow changes produced by the wave.

Nomenclature

a = gas sound speed
A_0, A_1, A_2 = coefficients for v_e, Eq. (24)
b_i = coefficients for T_W, Eq. (15)
C_B = wall specific heat
C_p, C_v = gas specific heats (const)
D = hydraulic diameter = 4 × cross section area/perimeter
$\operatorname{erf} c(z)$ = $[2/(\pi)^{1/2}] \int_z^\infty e^{-s^2} dS$
f_0, f_1, f_2 = constants in Eq. (24)
F = defined by Eq. (8)
g_0, g_1, g_2 = constants in Eq. (24)
G = defined by Eq. (9)
h = specific enthalpy $C_p T$
H = defined by Eq. (12)
k = coefficient of thermal conductivity
K = $(\rho_B C_B k_B)/(\rho_0 C_p k_0)$
p = gas pressure
q = heat-transfer rate, $-k \partial T/\partial y$
$\bar{q}$ = dimensionless heat-transfer rate defined by Eq. (22)
s = dimensionless independent variable, $x/(a_0 t)$
t = time measured relative to wave focus, $t' - t_0'$
t' = time measured relative to expansion wave origin
t_0' = time of wave focus, zero for expansion wave
T = gas temperature
ΔT = difference between stream and wall surface temperature, $T_e - T_W$
u = flow velocity along x' outside of boundary layer in tube-fixed coordinate system x', t'
$\bar{u}$ = flow velocity along x in x, y, t coordinate system attached to wavehead
v = flow velocity along y normal to the wall
x = distance from wavehead, $x' + a_0 t'$
x' = distance from expansion wave origin
y = distance normal to wall from wall-gas interface
α = thermal diffusivity of wall, $k_B/(\rho_B C_B)$
β = $2/(\gamma+1) = 1-\varepsilon$
γ = C_p/C_v, const
ε = $(\gamma-1)/(\gamma+1)$
η = $[a_0/(v_0 x)]^{1/2} \int_0 (\rho/\rho_0) dy$
$\bar{\eta}$ = $-y[a_0/(\alpha x)]^{1/2}$
θ = local temperature in the wall
μ = coefficient of viscosity of the gas
ν = kinematic viscosity of the gas, μ/ρ
ρ = mass density
σ = Prandtl number of the gas $\mu C_p/k$ = const
τ = shear stress $\mu \partial \bar{u}/\partial y$
$\bar{\tau}$ = dimensionless shear stress defined by Eq. (22)

Subscripts
B = denotes value for homogeneous wall material
e = denotes inviscid flow conditions in the absence of wall boundary layer
0 = denotes initial state of gas at rest ahead of wave
W = denotes conditions at gas-wall interface or $y = 0$

Received February 18, 1971; revision received September 7, 1971.
Index category: Boundary Layers and Convective Heat Transfer-Laminar.

* Professor, Department of Mechanical Engineering, and Director, Fluid and Thermal Sciences Laboratory. Member AIAA.

Introduction

THE present paper analyzes the unsteady laminar wall boundary layer formed within a finite expansion or compression wave traveling into a tube containing gas at rest, and the resulting displacement effects of the boundary layer on the unsteady inviscid flow in the tube interior. The type of flow in the expansion-wave case occurs, for example, in the high-pressure or driver section of a conventional shock tube after the diaphragm bursts (Fig. 1). A similar centered unsteady expansion-wave flow appears in the reservoir tube of a Ludweig or tube-type wind tunnel.[1] The type of flow in the compression-wave case might be similar to that generated by an accelerating piston (Fig. 2) such as employed in free-piston shock tubes[2] or isentropic compression tubes.[3] For both types of flow the extent